Low-moment antiferromagnetic ordering in triply charged cubic fullerides close to the metal-insulator transition

P. Jeglič,[1] D. Arčon,[1,2,*] A. Potočnik,[1] A. Y. Ganin,[3] Y. Takabayashi,[4] M. J. Rosseinsky,[3] and K. Prassides[4]
[1]*Institute "Jozef Stefan," Jamova 39, 1000 Ljubljana, Slovenia*
[2]*Faculty of Mathematics and Physics, University of Ljubljana, Jadranska 19, 1000 Ljubljana, Slovenia*
[3]*Department of Chemistry, University of Liverpool, Liverpool L69 7ZD, United Kingdom*
[4]*Department of Chemistry, Durham University, Durham DH1 3LE, United Kingdom*
(Received 1 September 2009; published 30 November 2009)

We report on the ambient pressure ^{13}C and ^{133}Cs NMR study of disorder-free A15-structured Cs_3C_{60}, which shows non-BCS superconductivity at 38 K under pressure. Temperature-independent ^{13}C and ^{133}Cs spin-lattice relaxation rates prove an insulating ground state with a small effective magnetic moment $1.3-1.6\mu_B$ for $T>100$ K. Below 46 K, A15 Cs_3C_{60} orders into an antiferromagnetic structure best described by a magnetic wave vector, $\mathbf{q}=(\frac{1}{2},\frac{1}{2},\frac{1}{2})$ with a staggered magnetic moment $\sim 0.9\mu_B$ per C_{60}. The large (U/W) ratio (~ 2.2), the opening of a gap in the electronic excitation spectrum and the small C_{60}^{3-} magnetic moment all underline the importance of electronic correlations in A15 Cs_3C_{60}.

DOI: 10.1103/PhysRevB.80.195424 PACS number(s): 76.60.−k, 74.70.Wz, 71.30.+h

The interplay between strong electron correlations and high-temperature superconductivity has been widely recognized but simple model systems to test key aspects of theory are currently missing. The alkali fulleride, Cs_3C_{60},[1] which is free of positional, chemical, and orientational disorder shows both a high T_c and a direct transition from an antiferromagnetic insulator (AFI) to a superconductor without any structural distortion.[2,3] The superconducting state emerges in the body-centered-cubic (bcc) based A15 phase directly from the ambient pressure AFI state with the application of pressure above 3.6 kbar.[2,3] T_c first increases with pressure but then exhibits a broad maximum at ~7 kbar where it reaches 38 K. The nonmonotonic dependence of T_c on pressure and the occurrence of superconductivity next to the AFI phase cannot be simply rationalized within the BCS formalism and highlight the importance of electronic correlations in A15 Cs_3C_{60}. This behavior is fundamentally different from that of the superconducting face-centered-cubic (fcc) A_3C_{60} phases, in which T_c increases monotonically with increasing interfulleride separation.[4]

The unconventional nature of the superconducting state emerging from the AFI state in A15 Cs_3C_{60} raises important generic questions about the interplay between magnetism and superconductivity and, in particular, how the proximity to the metal to insulator transition (MIT) boundary together with the single molecule properties, such as the Jahn-Teller effect and Hund's rule coupling, determine the A15 Cs_3C_{60} ground state. Investigations of the magnetic properties hold the key to the understanding of the role of electronic correlations, electron-phonon coupling and crystal symmetry in determining the ambient pressure AFI and high-pressure superconducting states. Here we report temperature-dependent ^{13}C and ^{133}Cs NMR measurements at ambient pressure on a powdered Cs_3C_{60} sample. Our results confirm the insulating ground state in A15 Cs_3C_{60} (Ref. 3) where t_{1u} electrons become localized due to the large (U/W) ratio (~2.2). Antiferromagnetic (AFM) order with a small staggered moment of $\sim 0.9\mu_B$ per C_{60}^{3-} unit is observed below $T_N=46$ K. The small magnetic moment in A15 Cs_3C_{60} arises either from the dynamic Jahn-Teller effect and/or because of the proximity to the MIT boundary. These findings are the hallmark of the importance of electronic correlations in expanded bcc-structured fullerides and provide a link between the anomalous pressure dependence of T_c and the ambient pressure AFI state in Cs_3C_{60}.

Synchrotron x-ray diffraction (XRD) showed that the studied Cs_3C_{60} batch contains predominantly A15 Cs_3C_{60} [52.2(1)%] with minority fcc Cs_3C_{60} [31.5(2)%] and body-centered orthorhombic (bco) $Cs_{3+x}C_{60}$ [16.3(2)%] phases. ^{133}Cs ($I=7/2$) and ^{13}C ($I=1/2$) NMR experiments were performed in a 8.9 T magnetic field. Reference frequencies, $\nu(^{13}C)=95.557$ MHz and $\nu(^{133}Cs)=49.845$ MHz were obtained from tetramethylsilane and $CsNO_3$ standards, respectively. In ^{13}C NMR line-shape experiments, a Hahn echo pulse sequence with $\pi/2=6$ μs was used. For ^{133}Cs NMR experiments we used a two-pulse $(\beta)-\tau-(\beta)-\tau-echo$ sequence; the pulse length, $\tau_\beta=2$ μs was optimized to amplify the A15 signal. A typical interpulse delay was $\tau=60$ μs. For spin-lattice relaxation time, T_1 measurements the saturation recovery technique was used. The repetition time was 0.2 s at ambient temperature.

Figure 1 shows the ^{13}C NMR powder spectra of Cs_3C_{60} for selected temperatures. The presence of different phases in the investigated sample is reflected in the multicomponent spectrum measured at 300 K [Fig. 1(a)]: a main sharp line (signal A) at 199 ppm, a broad background extending between 100(10) and 340(20) ppm (signal B) and a weak line centered at 180 ppm (signal C). The main signal A (relative intensity ~50%) is attributed to the dominant A15 polymorph following the assignment of Ref. 2 based on magic angle spinning ^{13}C NMR. Signals B and C are then due to the coexisting fcc and bco minority phases.

The above line-shape assignment allows us to follow the temperature dependence of the A15 ^{13}C NMR shift, $^{13}\delta_{iso}$, between 400 and 300 K. In this temperature range, $^{13}\delta_{iso}$ increases from 196 to 199 ppm with decreasing temperature [inset Fig. 2(a)]. In fullerides, $^{13}\delta_{iso}$ has two main contributions: the temperature-independent C_{60}^{3-} chemical shift, σ_{iso}

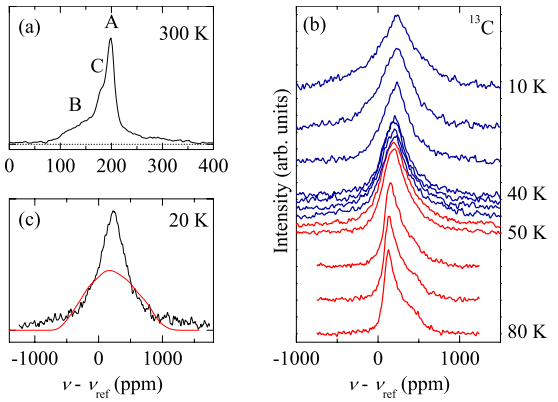

FIG. 1. (Color online) (a) ^{13}C NMR spectrum at 300 K. Signal A is due to the majority A15 Cs_3C_{60} phase while components B and C are due to the coexisting fcc Cs_3C_{60} and bco $Cs_{3+x}C_{60}$ phases. (b) Temperature evolution of the ^{13}C NMR spectra below 80 K. Note the sudden line shape change and broadening below 46 K. (c) ^{13}C NMR spectrum at 20 K. The thin solid red line is the calculated ^{13}C NMR line shape for the AFM2 structure, $\mathbf{q}=(\frac{1}{2},\frac{1}{2},\frac{1}{2})$ and $\mu_S=0.9\mu_B$. The narrow part of the spectrum not described by the fit is due to the coexisting fcc phase.

$=150$ ppm (Ref. 5) and the Fermi contact shift, $^{13}\delta_S$. $^{13}\delta_S$ is expressed with the hyperfine coupling constant, ^{13}A, and the uniform spin susceptibility, χ_S, as

$$^{13}\delta_S = \left(\frac{^{13}A}{\gamma_e \gamma_C \hbar}\right)\chi_S, \tag{1}$$

where γ_e and γ_C are the electron, and ^{13}C nuclear gyromagnetic ratios. Taking $^{13}\delta_S=49$ ppm and a typical C_{60}^{3-} value, $^{13}A/2\pi=0.69$ MHz,[6] we calculate the room-temperature spin susceptibility as $\chi_S=8.3\times10^{-4}$ emu/(mol C_{60}) from Eq. (1). Interpreting the increase in $^{13}\delta_{iso}$ with decreasing temperature as the signature of a Curie-Weiss behavior of χ_S with a Weiss constant, $\theta=-68$ K,[3] we can extract an effective moment, $\mu_{eff}\sim1.6\mu_B$. This is comparable to $\mu_{eff}=1.32(1)\mu_B$ extracted directly from the magnetic susceptibility data of an A15 sample with bco and fcc impurities.[3] It is also very close to $\mu_{eff}=1.73\mu_B$ expected for the localized $S=1/2$ spin state.

The *bco* $Cs_{3+x}C_{60}$ ^{13}C NMR signal can be easily separated from the other two spectral components below 300 K since it has much longer T_1. Therefore, spectra obtained in measurements with short repetition times are dominated by the rapidly relaxing A15 phase [Figs. 1(b) and 1(c)]. This allows us to accurately determine the temperature dependence of ^{13}C $1/T_1$ for cubic A15 (Ref. 3) and compare it with that of the orthorhombic antiferromagnetic insulators, $(ND_3)K_3C_{60}$ (Refs. 7 and 8) and $(CD_3ND_2)K_3C_{60}$, which differ in symmetry and unit-cell volume per C_{60}^{3-} (Fig. 3). For all three phases, $1/T_1$ is nearly temperature independent at high temperatures [a sudden decrease in $1/T_1$ in $(CD_3ND_2)K_3C_{60}$ is due to the structural phase transition at 220 K (Refs. 9 and 10)]. These results contradict the Korringa relation, $T_1T(\Delta K)^2=$const which is followed in metallic fcc A_3C_{60}.[11] The deviation from the Korringa relation and the similarity in $1/T_1$ with insulating $(ND_3)K_3C_{60}$ and $(CD_3ND_2)K_3C_{60}$

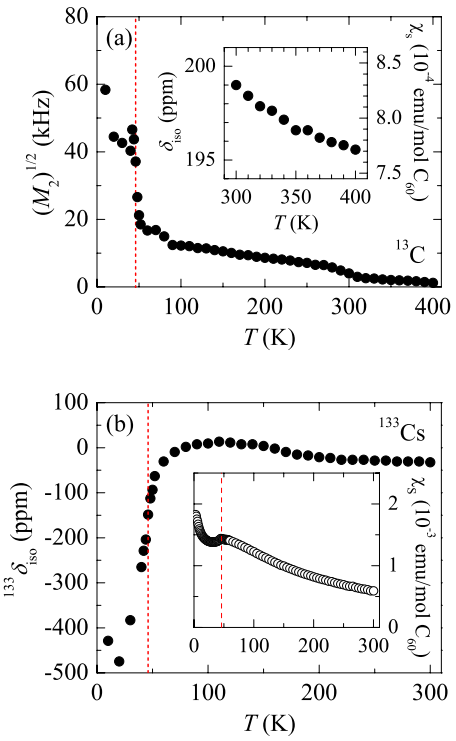

FIG. 2. (Color online) (a) Temperature dependence of the square root of the ^{13}C NMR second moment. Inset: A15 ^{13}C NMR shift (left scale) and the calculated χ_S (right scale) at high temperature. (b) Temperature dependence of the A15 ^{133}Cs NMR shift (solid circles). Inset: temperature dependence of the bulk χ_S (open circles) reproduced from Ref. 3. Vertical dashed lines mark $T_N=46$ K.

clearly rule out a metallic ground state for A15 Cs_3C_{60} and are fully consistent with the nuclear relaxation in exchange coupled antiferromagnetic insulators, where $1/T_1$ is in the high-temperature limit given by[12]

$$\frac{1}{T_1} = \sqrt{2\pi}\frac{^{13}A^2 + \frac{1}{2}A_{dip}^2}{3g^2\mu_B^2}\frac{\mu_{eff}^2}{\omega_{ex}}. \tag{2}$$

Here the dipolar hyperfine coupling constant is $A_{dip}/2\pi=3.38$ MHz (Ref. 6) and the exchange frequency $\omega_{ex}^2=2zk_B^2J^2S(S+1)/3\hbar^2$ is determined by the interfulleride exchange interactions, J, and the number of near neighbors in the bcc lattice, $z=8$, yielding $J/k_B=30$ K for A15 Cs_3C_{60}. Assuming antiferromagnetic exchange interactions, J can be expressed as $J=4t^2/U$, where t is the interfullerene transfer integral. For bcc lattice, $t\sim W/16$ and by taking a typical value for the on-site Coulomb repulsion, $U\sim1$ eV,[13,14] we estimate $W=0.43$ eV. The extracted bandwidth is essentially identical with that calculated, $W=0.49$ eV (Ref. 15) and implies that nonfrustrated A15 Cs_3C_{60} is insulating because of the large $(U/W)=2.2$ ratio.

We now turn to ^{133}Cs NMR, which is an established probe of local structural details through the quadrupolar interaction and of magnetic properties via electron-nuclear dipolar interactions. In the presence of quadrupole effects, the position of the central $\frac{1}{2}\leftrightarrow-\frac{1}{2}$ transition is unaffected to first order by

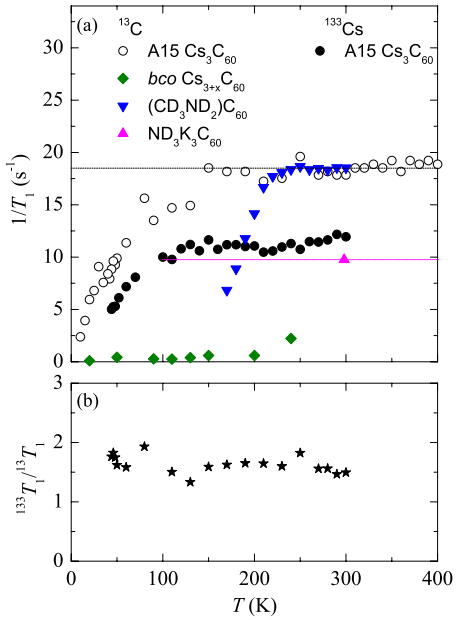

FIG. 3. (Color online) (a) Temperature dependence of the ^{13}C spin-lattice relaxation rate, $1/^{13}T_1$, in A15 Cs_3C_{60} (open circles), orthorhombic $(ND_3)K_3C_{60}$ (magenta upper triangle) and $(CD_3ND_2)K_3C_{60}$ (blue down triangles) phases. The A15 ^{133}Cs spin-lattice relaxation rate, $1/^{133}T_1$ is shown as black solid circles. Dotted lines are guides to the eye. (b) Temperature dependence of the ^{13}C and ^{133}Cs spin-lattice relaxation rates ratio, $^{133}T_1/^{13}T_1$.

the electric field gradient (EFG, $V_{ij}=\frac{\partial^2 V}{\partial x_i \partial x_j}$), while the shift of the satellite lines is proportional to a quadrupole frequency, $\nu_Q=\frac{3eQV_{zz}}{2I(2I-1)h}$, which is related to the strength of the EFG V_{zz} and the ^{133}Cs quadrupole moment, Q. Moreover, the structure of the EFG tensor is extremely sensitive to the local symmetry of the Cs site. For A15 Cs_3C_{60}, the site symmetry of the single Cs site ($-4m.2$) is compatible with uniaxial ($\eta=\frac{V_{xx}-V_{yy}}{V_{zz}}=0$) quadrupolar interaction. We optimized our pulsed echo sequence in order to obtain nearly pure A15 ^{133}Cs NMR spectra[3] with a typical $I=7/2$ quadrupole powder line shape [Fig. 4(a)]. A satisfactory agreement with the measured spectrum at 100 K can be achieved with $\nu_Q=39(1)$ kHz and $\eta=0$ [Fig. 4(a)].

In the line-shape analysis, we introduced a temperature-dependent ^{133}Cs NMR shift, $^{133}\delta_{iso}$ which first increases with decreasing temperature as expected for a paramagnetic insulator. The temperature-dependent part of the ^{133}Cs shift can be expressed as $^{133}\delta_S=(\frac{^{133}A}{\gamma_e\gamma_{Cs}\hbar})\chi_S$, where γ_{Cs} is the ^{133}Cs gyromagnetic ratio and ^{133}A is the corresponding hyperfine coupling constant. A linear relationship between $^{133}\delta_S$ and χ_S is obeyed between room temperature and ~120 K, yielding $^{133}A/2\pi=0.35(3)$ MHz. However, below ~120 K, $^{133}\delta_{iso}$ suddenly begins to shift to lower frequencies [Fig. 2(b)]. On the other hand, magnetic-susceptibility measurements[3] reveal no anomalous response and the bulk χ_S increases monotonically in this temperature range [inset to Fig. 2(b)]. Although the measured χ_S includes contributions from the coexisting fcc and bco phases, it appears unlikely that the anomalous temperature dependence of $^{133}\delta_S$ below ~120 K can be explained in terms of a sudden change in $\chi_S(T)$ and we therefore attribute it to a change in ^{133}A. As ^{133}A is given by the Fermi contact interaction due to the nonzero Cs $6s$ orbital admixture in the t_{1u} orbital and the core-polarization hyperfine coupling resulting from the exchange polarization of the Cs core electrons by unpaired C_{60}^{3-} electrons, a plausible explanation for the observed temperature dependence of $^{133}\delta_{iso}$ is that the Fermi contact interaction begins to change around 120 K. This change in the Fermi contact interaction may be associated with the onset of dynamic Jahn-Teller distortion at the C_{60}^{3-} anions on the time scale of our NMR experiments.

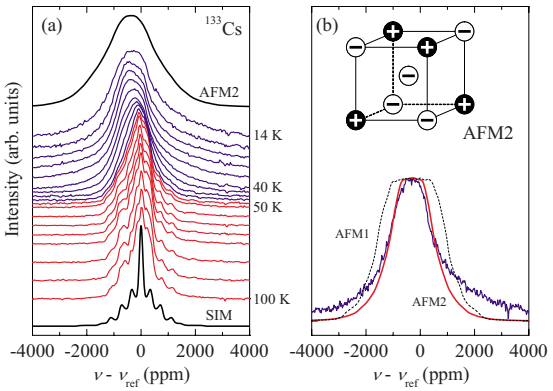

FIG. 4. (Color online) (a) Temperature dependence of the ^{133}Cs NMR powder spectra for A15 Cs_3C_{60}. For comparison we include the high-temperature fit of the quadrupolar powder spectrum with $\nu_Q=39$ kHz and $\eta=0$ (bottom) and the low-temperature fit for the AFM2 structure with $\mathbf{q}_2=(\frac{1}{2},\frac{1}{2},\frac{1}{2})$ (top). (b) Comparison between the experimental ^{133}Cs NMR spectrum at 14 K (thick blue line) and the calculated spectra for the AFM2 (solid red line) and AFM1 [$\mathbf{q}_1=(1,1,1)$, dashed black line] structures. In both simulations, $\mu_S=0.9\mu_B$.

Interestingly, ^{13}C $1/T_1$ also becomes gradually suppressed below ~120 K [Fig. 3(a)].[3] We stress that in this temperature range the C_{60}^{3-} units are already static on the ^{13}C NMR time scale and there is no structural phase transition that could account for the $1/T_1$ reduction. Therefore the observed temperature dependence of $1/T_1$ should reflect a change in the C_{60}^{3-} spin dynamics, described by the imaginary part of the spin susceptibility, $\chi''(\vec{q},\omega)$. Then the ^{13}C $1/T_1$ suppression is consistent with the opening of a small gap in the spin excitation spectrum at discrete points in $\vec{q}$ space so that $\chi''(\vec{q},\omega)\propto e^{-\Delta_q/T}$. We estimate that the wave-vector-dependent spin gap, Δ_q is on the order of 0.1 eV, which is a typical energy scale for the excitations induced by the dynamic Jahn-Teller effect.[16] At the same time, the temperature dependence of ^{133}Cs $1/T_1$ is nearly identical to that of ^{13}C $1/T_1$ [Fig. 3(a)]. Noting that ^{133}Cs $1/T_1$ (T) is determined in part by the temperature dependence of ^{133}A and in part by that of $\chi''(\vec{q},\omega)$, we conclude that the temperature-invariant $^{133}T_1/^{13}T_1$ ratio [Fig. 3(b)] reflects the dominant effect of $\chi''(\vec{q},\omega)$ on ^{133}Cs $1/T_1$. Therefore, the gap in the excitation spectrum detected in ^{13}C $1/T_1$ is additionally supported by the ^{133}Cs $1/T_1$ data and may be linked with the anomalous temperature dependence of $^{133}\delta_{iso}$. Since such a gap is not present in the low-symmetry large unit-cell volume $(ND_3)K_3C_{60}$ and $(CD_3ND_2)K_3C_{60}$ systems, we attribute it to

a specific property of the insulating A15 state close to the MIT boundary.

At temperatures below 46 K, the ^{13}C NMR signal suddenly becomes very symmetric and broadens with decreasing temperature [Figs. 1(b) and 1(c)] leading to a dramatic increase in M_2 [Fig. 2(a)]. At the same time, the ^{133}Cs NMR line shape also dramatically broadens,[3] becomes more symmetric and the details of the quadrupole line-shape structure are lost [Fig. 4(b)]. The ^{133}Cs NMR spectra continuously broaden on cooling below 46 K and the ^{133}Cs NMR second moment follows the magnetic order parameter, unambiguously confirming the AFM ordering of the A15 phase.[3]

We now proceed to address the low-temperature magnetic structure of the A15 phase by simulating the ^{133}Cs NMR spectra using the formalism developed earlier for ammoniated and methylaminated alkali fullerides[8,10] and A_1C_{60}.[17] The orientation of a staggered magnetic moment, μ_S, placed at the center of the C_{60} molecule, was calculated in the spin-flop phase (the spin-flop field is usually on the order of only 100 mT in fullerides[9]). For simplicity only collinear magnetic structures are considered. Two possible magnetic structures, which are compatible with the bcc symmetry[18] are described by ordering vectors $\mathbf{q}_1=(1,1,1)$ (AFM1) and $\mathbf{q}_2=(\frac{1}{2},\frac{1}{2},\frac{1}{2})$ (AFM2). Which of the two magnetic structures will prevail depends on the relative strength of the first-nearest-neighbor (J_1) and second-nearest-neighbor interactions (J_2). There is a quantum phase transition from AFM1 to AFM2 at $J_2/J_1=0.705$.[18] Best agreement between experimental and simulated spectra [solid line in Fig. 4(b)] was obtained for the AFM2 structure [inset Fig. 4(b)] with $\mu_S=0.9\mu_B$. As a consistency check, we also calculated the ^{13}C NMR line shape [Fig. 1(c)] and found an acceptable agreement. The simple AFM1 structure with the same μ_S results in a ^{133}Cs NMR line, that is, broader than the experimental spectrum [dashed line in Fig. 4(b)]. In order to match the experimental spectrum, a reduced $\mu_S=0.6\mu_B$ has to be used. Although our results cannot unambiguously distinguish between the two magnetic structures, they point to a small staggered moment of less than $1\mu_B$ per C_{60}^{3-}. The alternative disordered magnetic moment ground state is in disagreement with both the observation here that M_2 increases sharply at the ordering temperature and with ZF-μSR measurements[3] which find a long-range magnetically ordered ground state.

Our ^{13}C and ^{133}Cs NMR results provide additional evidence for the ambient-pressure AFI ground state of A15 Cs_3C_{60}.[3] An important finding of the present work is the reduced magnitude of the magnetic moment: in the paramagnetic phase, $\mu_{eff}=1.3-1.6\mu_B$, while in the AFM phase, $\mu_S=0.6-0.9\mu_B$. For a system, that is, deep in the Mott insulating state, the t_{1u} electrons are localized on each C_{60} unit and result in either a high-spin (HS) $S=3/2$ or a low-spin (LS) $S=\frac{1}{2}$ state. The measured μ_{eff} is significantly smaller than the HS value and much closer to that of the LS state. This implies that in A15 Cs_3C_{60} the LS state, stabilized by the Jahn-Teller effect, narrowly prevails over the HS state favored by the interorbital Hund's rule exchange and the observed gap is due to the energy difference between these two states. However, the Jahn-Teller effect has to be dynamic since our XRD studies show that cubic symmetry is maintained down to 4 K.[3] The diamagnetic shift of $^{133}\delta_{iso}$ is then presumably related to the broken orbital rotational symmetry on the NMR time scale. The long-range orbital-ordering temperature with static Jahn-Teller molecular distortions should be very low. For instance, in monoclinic TDAE-C_{60}, Jahn-Teller dynamics freeze below 9 K.[19–22] This scenario is in agreement with recent theoretical investigations underlying the importance of electronic correlations and the dominance of the dynamic Jahn-Teller effect in cubic fullerides close to the MIT boundary.[23] An alternative explanation for the reduced magnetic moment could be based purely on the proximity of A15 Cs_3C_{60} to the MIT border. In this context, the magnetic susceptibility of narrow-band electron systems is expected to obey the Curie-Weiss law for a wide range of U (Ref. 24) but local excitations can dramatically renormalize the values of μ_{eff} and μ_S when the system with large U/W is in the vicinity of the MIT boundary. Further theoretical and experimental investigations are needed to distinguish between these two models.

In conclusion, the NMR results are consistent with an ambient pressure insulating ground state for A15 Cs_3C_{60}, which orders antiferromagnetically below $T_N=46$ K with a reduced staggered magnetic moment of $\sim 0.6-0.9\mu_B$ per C_{60}^{3-}. The most likely magnetic structure is described by the magnetic wave vector $\mathbf{q}=(\frac{1}{2},\frac{1}{2},\frac{1}{2})$ and suggests the importance of interfulleride exchange coupling not only between first but also between second nearest C_{60}^{3-} neighbors. The small C_{60}^{3-} magnetic moments, the large $(U/W)=2.2$ ratio, and the small gap in the electronic excitation spectrum reflect the importance of the electronic correlations in alkali-doped fullerides with expanded unit cells.

We thank the EPSRC (Grants No. EP/G037132 and No. EP/G037949) for financial support (M.J.R./K.P.).

*denis.arcon@ijs.si

[1] T. T. M. Palstra, O. Zhou, Y. Iwasa, P. E. Sulewski, R. M. Fleming, and B. R. Zegarski, Solid State Commun. **93**, 327 (1995).
[2] A. Y. Ganin, Y. Takabayashi, Y. Z. Khimyak, S. Margadonna, A. Tamai, M. J. Rosseinsky, and K. Prassides, Nature Mater. **7**, 367 (2008).
[3] Y. Takabayashi, A. Y. Ganin, P. Jeglič, D. Arčon, T. Takano, Y. Iwasa, Y. Ohishi, M. Takata, N. Takeshita, K. Prassides, and M. J. Rosseinsky, Science **323**, 1585 (2009).
[4] See, for instance, S. Margadonna and K. Prassides, J. Solid State Chem. **168**, 639 (2002).
[5] Y. Maniwa, D. Sugiura, K. Kume, K. Kikuchi, S. Suzuki, Y. Achiba, I. Hirosawa, K. Tanigaki, H. Shimoda, and Y. Iwasa, Phys. Rev. B **54**, R6861 (1996).
[6] N. Sato, H. Tou, Y. Maniwa, K. Kikuchi, S. Suzuki, Y. Achiba, M. Kosaka, and K. Tanigaki, Phys. Rev. B **58**, 12433 (1998).

[7] K. M. Allen, S. J. Heyes, and M. J. Rosseinsky, J. Mater. Chem. **6**, 1445 (1996).
[8] H. Tou, Y. Maniwa, Y. Iwasa, H. Shimoda, and T. Mitani, Phys. Rev. B **62**, R775 (2000).
[9] D. Arčon, M. Pregelj, A. Zorko, A. Yu. Ganin, M. J. Rosseinsky, Y. Takabayashi, K. Prassides, H. van Tol, and L.-C. Brunel, Phys. Rev. B **77**, 035104 (2008).
[10] D. Arčon, A. Y. Ganin, Y. Takabayashi, M. J. Rosseinsky, and K. Prassides, Chem. Mater. **20**, 4391 (2008).
[11] C. H. Pennington and V. A. Stenger, Rev. Mod. Phys. **68**, 855 (1996).
[12] T. Moriya, Prog. Theor. Phys. **16**, 23 (1956).
[13] O. Gunnarsson, *Alkali-doped Fullerides. Narrow-Band Solids with Unusual Properties* (World Scientific, Singapore, 2004).
[14] J. E. Han, O. Gunnarsson, and V. H. Crespi, Phys. Rev. Lett. **90**, 167006 (2003).
[15] G. R. Darling, A. Y. Ganin, M. J. Rosseinsky, Y. Takabayashi, and K. Prassides, Phys. Rev. Lett. **101**, 136404 (2008).
[16] V. Brouet, H. Alloul, Thien-Nga Le, S. Garaj, and L. Forro, Phys. Rev. Lett. **86**, 4680 (2001).
[17] V. Brouet, H. Alloul, Y. Yoshinari, and L. Forro, Phys. Rev. Lett. **76**, 3638 (1996).
[18] J. Oitmaa and W. Zheng, Phys. Rev. B **69**, 064416 (2004).
[19] R. Blinc, P. Jeglič, T. Apih, J. Seliger, D. Arčon, and A. Omerzu, Phys. Rev. Lett. **88**, 086402 (2002).
[20] P. Jeglič, R. Blinc, T. Apih, A. Omerzu, and D. Arčon, Phys. Rev. B **68**, 184422 (2003).
[21] D. Arčon, J. Dolinšek, and R. Blinc, Phys. Rev. B **53**, 9137 (1996).
[22] R. Blinc, J. Dolinšek, D. Arčon, D. Mihailovič, and P. Venturini, Solid State Commun. **89**, 487 (1994).
[23] M. Capone, M. Fabrizio, C. Castellani, and E. Tosatti, Rev. Mod. Phys. **81**, 943 (2009).
[24] T. Moriya and H. Hasegawa, J. Phys. Soc. Jpn. **48**, 1490 (1980).